

Beam losses, energy deposition and residual gas pressure dynamics for different positions of the SIS90 collimators

C. Omet, K. Blasche, A. Krämer, J. Stadlmann and P. Spiller

October 6, 2005

Abstract

This note summarizes the results of simulations on the planned operation of SIS90 with intermediate charge-state-ions (U^{28+}). Especially the optimum position of the charge collimators for the control of beam losses produced by charge-exchange-processes like $U^{28+} \rightarrow U^{29+}$ has been determined.

For two different positions of the collimation system which has been discussed, in front of the quadrupoles and in between quadrupoles, the maximum dynamic residual gas pressure, the U^{28+} beam losses, the energy deposition in the walls and in the collimators per acceleration cycle are presented. The pumping properties of the cold surfaces and the reduction of pumping speed had been considered.

1 Positioning of the catchers in the SIS90 lattice

The SIS90 collimation system consists of 48 wedge-shaped collimators as described in [1]. In each of the 6 arcs 8 collimators are placed between the defocusing ("D") and the focusing ("F") quadrupole. This position leads to a high collimation efficiency (ratio of charge-exchanged ions which hit the collimators, not the wall) for the charge-exchange $U^{28+} \rightarrow U^{29+}$, but a decreasing collimation efficiency for multiple ionization (e.g. $U^{28+} \rightarrow U^{30+}$).

To improve this situation, a position of the collimators in front of the "D" quadrupole was proposed by A. Kovalenko et. al. [2]. This position results in a lower collimation efficiency for U^{29+} , but increasing collimation efficiencies for multiple ionization (e.g. U^{30+}), see tab. 1.

Table 1: Collimation efficiencies of the SIS90 collimation system for different collimator positions and ion types; calculated with "StrahlSim" [3].

collimator position	U^{27+}	U^{29+}	U^{30+}	U^{31+}
between quadrupoles	0 %	80.80 %	43.17 %	29.40 %
in front of quadrupoles	0 %	58.32 %	44.37 %	42.15 %

The SIS90 lattice has a high momentum acceptance, so the charge-exchanged ions have a probability greater zero to survive a full turn. This probability has been calculated with the "StrahlSim" code [3] and is shown in tab. 2.

Table 2: Storage probability of the SIS90 for different ion types

ion type	U^{27+}	U^{29+}	U^{30+}	U^{31+}
storage probability	3.33 %	24.25 %	1.66 %	1.53 %

2 Considerations

All charge-exchange cross sections of U^{28+} were taken from Olsen [4] and exponentially extra-/interpolated over the full energy range of SIS90. The data show that the charge-exchange cross section for $U^{28+} \rightarrow U^{30+}$ at high energies is about one order of magnitude lower than the one for $U^{28+} \rightarrow U^{29+}$.

During the injection time of 1 s, systematic beam losses of 10 % are considered (e.g. by incoherent tune shift [5]). For each simulation, the horizontal position of the collimator was chosen exactly at the acceptance limit of the machine (no reduction of the acceptance). The working point was chosen to be $Q_h = 19.x$ and $Q_v = 17.y$.

2.1 Acceleration cycle

The standard acceleration cycle of SIS90 assumes injection of four bunches ($2.5 * 10^{11}$ particles each) from the existing SIS18 at an energy of 96...192 MeV/u (all following calculations were done with 192 MeV/u). SIS18 requires 0.35 s for acceleration, leading to a total storage time of about 1 s in SIS90. After injection of $1 * 10^{12}$ particles, acceleration to 2.375 GeV/u with a ramp rate of 4 T/s is planned.

2.2 Vacuum properties and pumping power

The SIS90 consists of about 218 m of warm ($T = 300K$) and 865 m cold ($T < 20K$) sections. The total surface area of SIS90 is the sum of the cold and warm sections and estimated to be $A = A_{warm} + A_{cold} = 65.9m^2 + 261.4m^2 = 327.3m^2$.

2.2.1 Warm sections

In the warm sections, a combination of 48 ion sputter pumps and titanium sublimation pumps with an assumed effective pumping speed of $S_{eff,pump} = 1250l/s$ each leads to a total effective pumping speed of $S_{eff,warm} = 60m^3/s$. The specific outgassing rate of the baked stainless-steel vacuum chambers is assumed to be $q = 4.0 * 10^{-13} mbar * l / (s * cm^2)$, wich leads to a minimum pressure of $p_{end} = Q/S_{eff} = q * A/S_{eff} = 4.4 * 10^{-12} mbar$.

The vacuum composition in the warm sections was assumed to consist of 90 % H_2 , 9 %

CH_4 and 1 % CO according to measurements taken in SIS18 section S03 [6]. This data shows no heavy components like Ar and Cl .

2.2.2 Cold sections

The cold surfaces are assumed to pump with a specific pumping speed of $S_A = 1.25l/(s * cm^2)$, which leads to a total pumping speed of $S_{eff,cold} = 3267.4m^3/s$. The area specific outgassing rate of to cold surfaces is very small and estimated to be $q = 1 * 10^{-15}mbar * l/(s * cm^2)$ or smaller, which leads to an unmeasurable minimum pressure of $p_{end} = 8 * 10^{-16}mbar$.

In case much more than a monolayer of gas has been frozen out on the surface, the pumping power of the cold surfaces will decrease. In this case we assume the pumping speed is reduced by a factor of 5, which leads to a minimum pressure of $p_{end} = 4 * 10^{-15}mbar$.

The vacuum composition in the cold sections is dominated by He , followed by H_2 and Ne . The exact values are not important as it is shown below.

2.3 Average pressure and pumping speed

The simulation code uses only the ring averaged pressure and pumping speeds (this is a valid simplification, because all considered beam losses are linear in pressure), so the above calculated values have to be weighted with the cold and warm section length ratio. The following cases had been assumed:

- UHV-case 1: (directly after cooling down), $S_{eff} = 2621.2m^3/s$, initial pressure $p_0 = 8.86 * 10^{-13}mbar$ ($8.86 * 10^{-11}Pa$)
- UHV-case 2: (after several weeks of operation), $S_{eff} = 533.9m^3/s$, initial pressure $p_0 = 8.89 * 10^{-13}mbar$ ($8.89 * 10^{-11}Pa$)

The average initial pressures differ not much, because they are dominated by the pressure in the warm section. The vacuum composition of the warm section therefore is taken into account only, instead of mixing both cold and warm constituents.

3 Simulation results

Three different options had been studied:

- a) without collimators
- b) with collimators between the "D" and "F" quadrupole (abbrev. DCF)
- c) with collimators in front of the "D" quadrupole (abbrev. CDF)

The simulations were performed with the "StrahlSim" code [3], which is capable to calculate the absolute particle losses, the residual gas pressure and the total energy

deposited in the walls and in the collimators with coulomb-scattering, charge-exchange-processes and desorption effects including collimators and storage probability. It could be shown that the 10 % systematic losses during injection do not trigger any additional charge-exchange-caused losses.

3.1 Particle losses

Fig. 1 and 2 show the time-resolved evolution of the number of particles for a full SIS90 cycle; for UHV-case 1 there is no noticeable difference between a) with and without collimators, no matter in which position they are placed. The effect of the collimator system is very small.

In UHV-case 2 without collimators the avalanche-effect (which was already observed at high-current-operation in SIS18, limiting there the maximum reachable intensity) is indicated. With collimators, this effect is reduced to a large extend.

The simulation shows that the absolute number of particles after acceleration (see tab. 3) is slightly dependent on the collimator position for both UHV-cases 1 and 2. The dynamic vacuum pressure is plotted in fig. 3/4.

Table 3: Maximum pressure, number of lost ions and final number of particles in SIS90 after acceleration for different collimator positions and UHV conditions.

UHV-case	options	N_{end}	losses	losses / %	\hat{p} / mbar
1	without coll.	$8.859 * 10^{11}$	$1.142 * 10^{11}$	11.42	$1.004 * 10^{-12}$
1	with coll., DCF	$8.864 * 10^{11}$	$1.136 * 10^{11}$	11.36	$9.733 * 10^{-13}$
1	with coll., CDF	$8.864 * 10^{11}$	$1.137 * 10^{11}$	11.37	$9.716 * 10^{-13}$
2	without coll.	$7.567 * 10^{11}$	$2.434 * 10^{11}$	24.34	$5.896 * 10^{-11}$
2	with coll., DCF	$8.819 * 10^{11}$	$1.182 * 10^{11}$	11.82	$1.333 * 10^{-12}$
2	with coll., CDF	$8.802 * 10^{11}$	$1.198 * 10^{11}$	11.98	$1.527 * 10^{-12}$

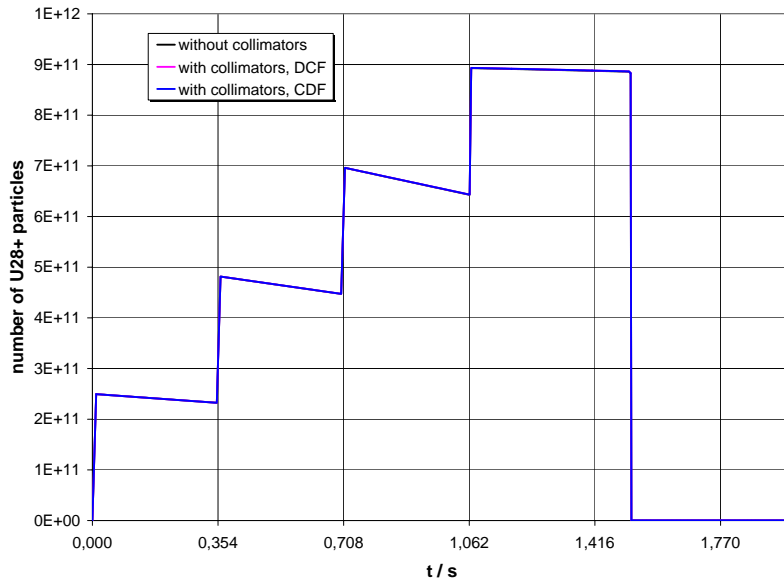


Figure 1: Time resolved simulation of the number of particles in SIS90 for different collimator positions for UHV-case 1. Note: No noticeable difference for the different options is expected.

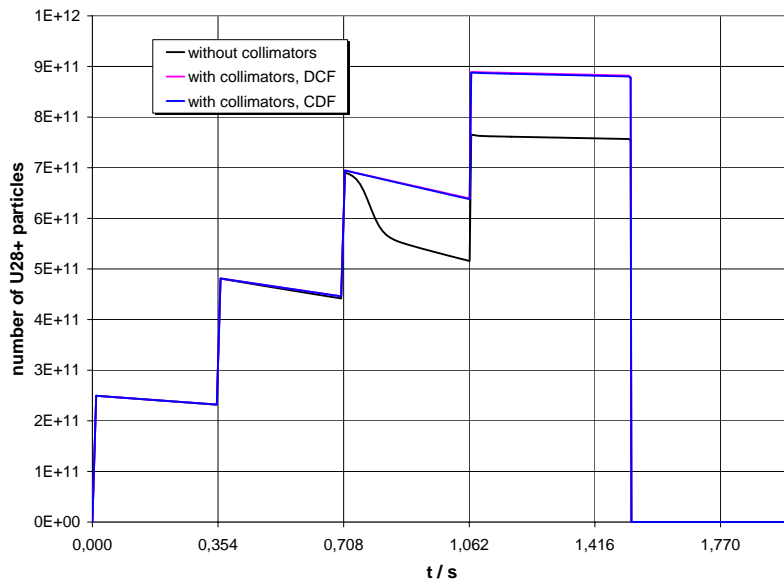


Figure 2: Time resolved simulation of the number of particles in SIS90 for different collimator positions for UHV-case 2.

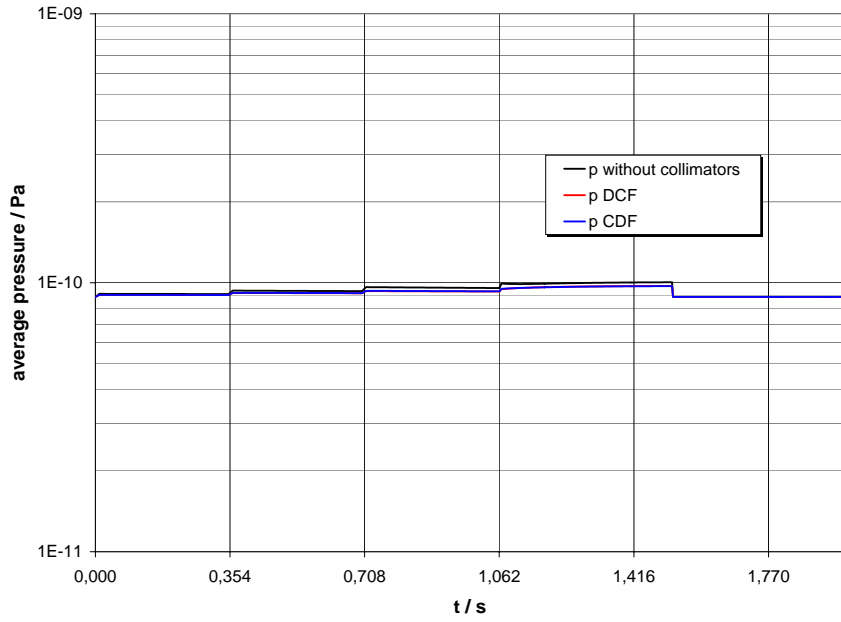


Figure 3: Average pressure evolution over time in Pa for UHV-case 1.

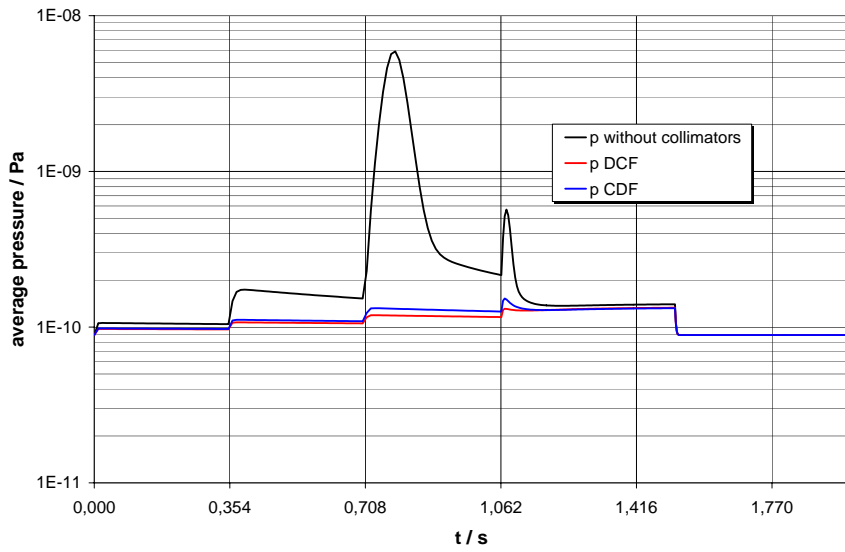


Figure 4: Average pressure evolution over time in Pa for UHV-case 2. Note the different scaling to fig. 3

3.2 Energy deposition

The energy deposition by lost beam ions over a full cycle is plotted in fig. 5/6 and summarized in tab. 4. It is assumed that the systematic losses will be captured in a dedicated halo collimation system in the warm straight sections, while the uncontrolled losses are deposited in the cold walls. Only the uncontrolled losses will cause a heat load to the SIS90 cryogenic system. The charge collimators are proposed to be cooled with liquid- N_2 to about 80 K.

Table 4: Energy deposition in different SIS90 systems, averaged over a full SIS90 cycle.

UHV-case	options	$E_{halocoll.@300K}$ / W	$E_{wall@20K}$ / W	$E_{coll.@80K}$ / W
1	without coll.	0.372	0.208	-
1	with coll., DCF	0.372	0.126	0.079
1	with coll., CDF	0.372	0.118	0.087
2	without coll.	0.372	0.671	-
2	with coll., DCF	0.372	0.128	0.093
2	with coll., CDF	0.372	0.134	0.100

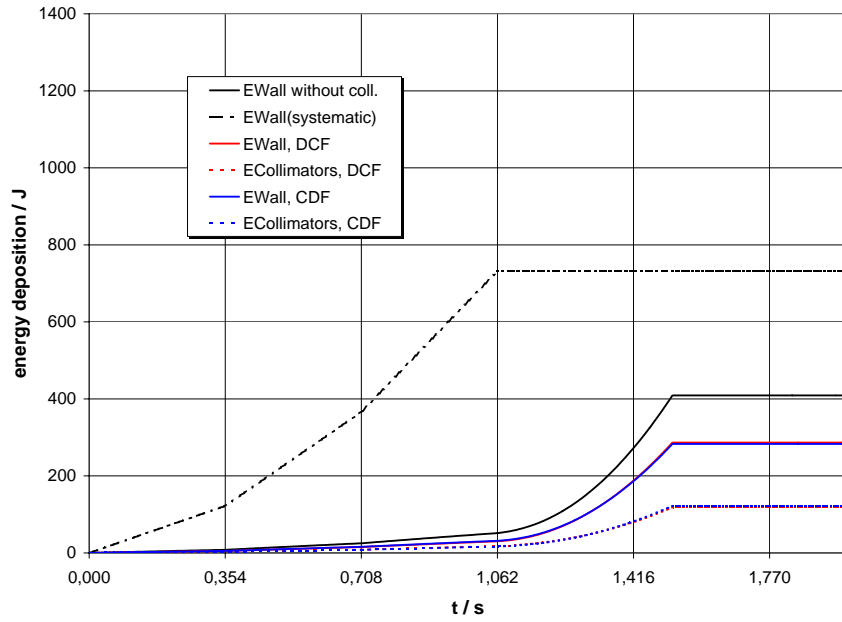


Figure 5: Energy deposition in J in halo collimators (systematic), cold wall and desorption collimators for UHV-case 1.

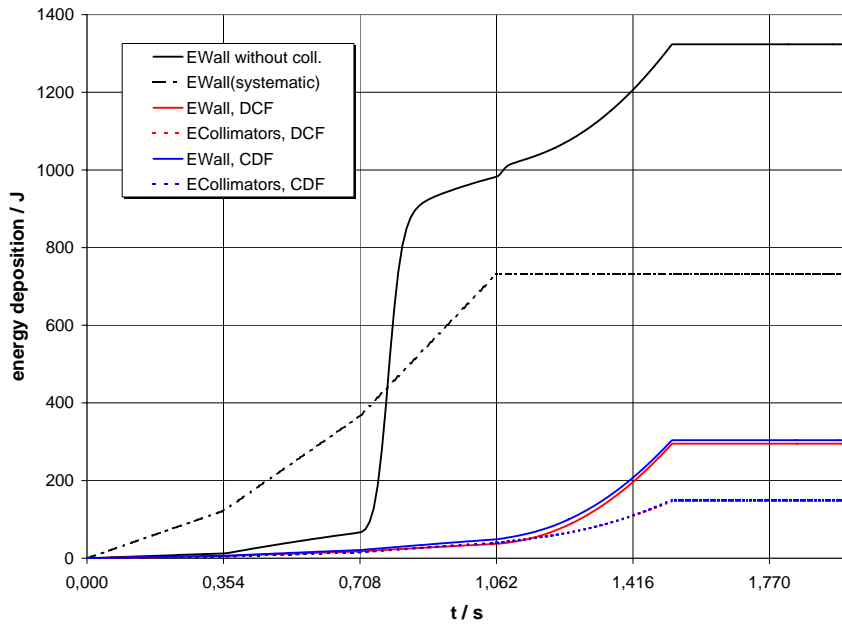


Figure 6: Energy deposition in J in halo collimators (systematic), cold wall and desorption collimators for UHV-case 2.

4 Conclusions

$a \lesssim 8$ At high pumping speeds, the total beam losses by charge exchange processes and energy deposition are not significantly different for the two collimator positions. In this case the collimation system has only a small effect at all. Nevertheless, at high energy and shallow angles, a cold surface can have very high desorption yields (up to $\eta = 1 * 10^7$ were measured at RHIC [7]). This fact was neglected completely in the simulation by choosing a more conservative $\eta = 4.5 * 10^4$.

Furthermore, the pumping speed may be drastically reduced after freezing out one or more monolayer of gas on the cold surface. This may already be the case after the first cooling down due to insufficient pre-pumping or due to gas desorption or outgassing after several weeks of operation. Important for the later process is the ratio between warm and cold surfaces in the synchrotron.

It was assumed that the pumping power is reduced due to frozen gases by a factor of five. For this case the collimator position between the quadrupoles is the most proper one as can be seen from fig. 7 and leads to a stabilization of the dynamics of the residual gas pressure.

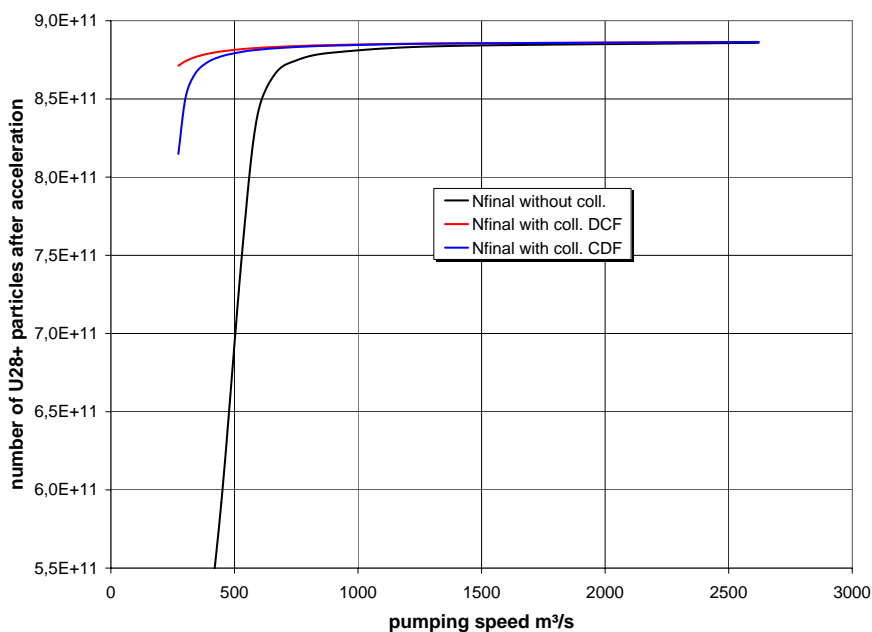


Figure 7: Simulation of the final number of particles after acceleration in SIS90 for different collimator positions.

References

- [1] C. Omet. *Auslegung eines Kollimatorsystems zur Lokalisierung von Umladungsverlusten und Beseitigung von Desorptionsgasen hochenergetischer, intensiver Schwerionenstrahlen in Ringbeschleunigeranlagen*. Diplomarbeit, Technische Universität Darmstadt, 01 2005.
- [2] A. Kovalenko. final report contract C1/AC No. 2. Report, JINR, 2005.
- [3] C. Omet. Verlustrechnungen für Ionenstrahlen unter dynamischem Vakuum in Ringbeschleunigern. *GSI Internal Report GSI-Acc-Report-2004-12-001*, 2004.
- [4] R. E. Olsen. Projectile Electron Loss and Capture in MeV/u Collisions of U28+ with H2, N2 and Ar. *Phys. Lett., B*, 2004.
- [5] G. Franchetti. Private communication.
- [6] UHV Group GSI. BES.101103.UHV. GSI Accelerator Report, GSI, 2003.
- [7] S.Y. Zhang. Ion Desorption at RHIC. In *High Intensity and High Brightness Hadron Beams*, number 773 in AIP Conference Proceedings, pages 216–218. American Institute of Physics, 10 2004.